ELSEVIER

International Journal of Mass Spectrometry 206 (2001) 211–229

International Journal of Mass Spectrometry

Ion-optical properties of time-of-flight mass spectrometers

Damaschin Ioanoviciu

National Institute for Research and Development of Isotopic and Molecular Technologies, P.O. Box 700, Ro 3400 Cluj-Napoca, Romania

Received 10 January 2000; accepted 2 August 2000

Abstract

The time focusing properties of time-of-flight mass spectrometers in current use, under development, or with probable future applications are presented. For most of the presented analyzer types a mass resolution formula was given to calculate instrumental performance. These formulas account for second or third order contributions to the ion packet length, depending upon the analyzer's focusing degree. This analysis covers homogeneous electric field mirrors, cylindrical reflectrons, quadratic potential mirrors with and without field free spaces included, linear drift space focusing analyzers, as well as quadrupole trap time-of-flight hybrid systems. The velocity focusing procedures by delayed extraction and postsource focusing, very useful in matrix-assisted laser desorption/ionization time-of-flight mass spectrometry, are also detailed. (Int J Mass Spectrom 206 (2001) 211–229) © 2001 Elsevier Science B.V.

Keywords: TOF mass spectrometers; Ion optics; Time focusing; Velocity focusing; Energy focusing

1. Introduction

The outstanding features of the time-of-flight mass spectrometers (TOFMSs) were already revealed by Wiley and McLaren [1]. They provide high sensitivity, allow complete mass spectrum detection from each ion packet, and their mass range is unlimited. In fact, the mass range is determined by the time lapse between the emission of two successive packets and by the lowest ion velocity still allowing detection. Only ions having velocities higher than 10 000 m/s can be "seen" by a channel plate or an electron multiplier detector [2]. Therefore the highest detectable mass is related to the highest available ion accelerating voltage. Because matrix-assisted laser desorption/ionization (MALDI) became an ionization method, molecular ions of very high mass can be obtained. The mass range of TOFMS with MALDI sources extends beyond a 1 000 000 Da [3]. To unambiguously identify such high mass ions, comparable figures for mass resolution would be desirable. For the time being, even after the recently accomplished progress TOFMS can not yet satisfy this demand. However if in 1989 the highest resolution of TOFMS was 35 000 [4] recently resolutions over 55 000 were reported [5,6].

There are, in principle, two ways to increase TOFMS resolution: by ensuring better focusing or/and by increasing the mass dispersion. "Longitudinal" here means "along the ion path." In other words, to make the ion packet thinner measured along its flight direction and to increase the distance between two different ion mass packets at the detector. The final longitudinal ion packet size depends on the analyzer's ability to focus ions formed in different ion source points, with different velocities, at a different time.

PII S1387-3806(00)00314-6

The TOF analyzer's focusing properties are described by the behaviour of the various ions related to the motion of a reference particle. Constant electric fields can ensure focusing of ions created on different equipotential surfaces in the ion source. Electric fields changing in time (established suddenly at some determined instant) can focus ions with different individual initial velocities and/or formed at distinct instants. Both focusing actions cannot be obtained simultaneously by fields independent of time [7]. Therefore, the mass analyzer is chosen to focus the initial distribution that dominates or seeks a compromise when there is no obvious choice. Ions are created with some initial velocity component along the extracting field of the ion source. This field is constant or it is applied from a certain moment referred to as the beginning of the ionization process. If the field is homogeneous, the time the ion spends before leaving the extracting region [8] depends linearly on the initial velocity. The action of this term can be corrected by time dependent fields applied after the ion formation inside (delayed extraction) [9–16] or outside the source [postsource focusing (PSF)] [17]. Constant fields can ensure energy focusing compensating for ion energy differences resulting from different initial positions inside the extracting field.

The dominating initial parameter type is connected intimately with the ionization method. In a traditional electron bombardment ionization source the ions result in the ribbon of ionizing electrons. The created ion inherits the initial velocity of the sample gaseous molecule from which it originates. The most probable velocities correspond to energies of about 0.025 eV whereas extracting fields are of the order of 300 V/cm acting over ionizing electron ribbons of 1–2 mm wide.

The energy distribution of the secondary ions resulted from primary ion bombardment [secondary ion mass spectrometry (SIMS)] has the maximum of around 5 eV for elements and around 2 eV for molecules [18]. These are emitted from an electrode surface, often a plane surface. In this case, velocity focusing seems to best address this kind of distribution. However, energy focusing keeps final packet size between convenient limits to reach resolutions well above 10 000 [19].

In MALDI sources, usually ions, are generated by laser shots from surfaces located perpendicularly to the ion flight direction. The ions are generated from a plane surface with high initial velocities. Roughly, matrix and analyte ions gain similar velocities. The plume expanding after the laser shot whirls together analyte and matrix neutral molecules and ions. The ion velocity distributions have maxima from 500 m/s [20] to 1000 m/s [21,22] with full width at half maximum (FWHM) of 560 m/s. These maxima do not reveal obvious mass dependence. The ion velocity distribution at some stage of the plume expansion is difficult to relate to that at the moment when ions leave the surface. Collision phenomena and coulombian repulsive forces could modify the initial distribution. For direct mass analysis of MALDI ions, velocity focusing by delayed extraction is imperiously needed. Even so, the resolution worsens with increasing mass and there are two possible reasons for that: the effect of uncanceled higher order velocity aberrations (as the ratio of initial velocity to the velocity acquired by acceleration increases) or due to a different effect of the extracting field on the ions involved in the expanding process of the plume (however for higher masses, as longer delays are used, the plume is in a more advanced expansion state).

Ion packets can be formed from MALDI created ions also if they are directed first to a cooling cell [23] (rf only quadrupole filters represent an elaborate solution). The ions having energies less than about 10 eV are focused transversally and fill in an equipotential extraction space. The ion packets are produced by periodical extraction by a transversal electric field after each chamber filling. The ions of the packet then have a narrow distribution of the velocity components along the accelerating field. Because the depth of the chamber is around 3 mm, space, focusing is necessary. Similar focusing conditions are to be accounted for after orthogonal injection for electrospray created ions [24].

2. Homogeneous electric field mirrors

The formulas presented cover the theory developed in [25] and also the effect of a postaccelerating gap

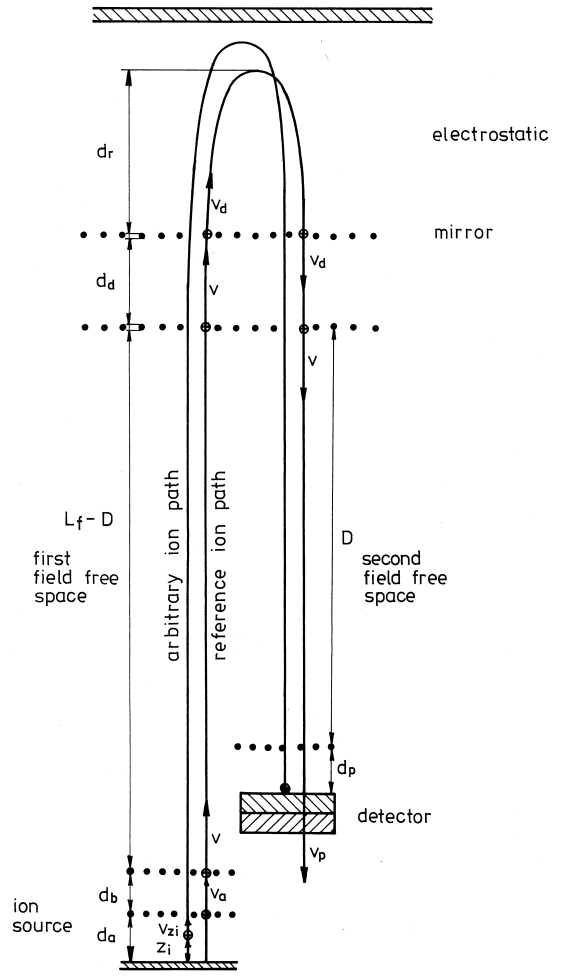

Fig. 1. Basic geometric parameters of a homogeneous electric field double stage reflectron.

being present. The extracting field acts on the ion of initial longitudinal velocity component v_{z_i}, and initial coordinate z_i, measured from a reference plane, located at d_a from this region exit's grid (Fig. 1). The accelerating field is applied on an interval d_b. Next, the ion flies on the field free space of length $L_f - D$ before entering the mirror's decelerating field. The decelerating field acts on a stage of d_d width before the ion enters the reflecting field stage. There the field acts inside that stage of depth of at least d_r. In fact this stage must be deeper to allow ions of energies higher than the reference ion to be returned. After reflection the ion leaves the mirror and moves over to the D field free space before reaching the postaccelerating field, applied inside the gap d_p. The motion of some ion is described with respect to a reference ion. The reference ion is selected to have mass m, charge q, starting without initial velocity from the origin of the longitudinal coordinate, at the moment when an ionization, packet generation-analysis detection cycle begins. The ion motion derivations given here neglect the incidence angle (same as the emergence angle) made by the packet axis at the mirror's entry plane. For realistic designs, this angle is often less than 2° and the resulted aberrations are irelevant for the usual resolutions [26]. However, these aberrations are of interest for high resolutions and they can be calculated with the formulas of [27] and [28] (where the detector oblique position is accounted for).

To build a mass resolution formula, the flight times of the above-mentioned ion path sequences are needed. The ion velocities and flight times were detailed with the formulas of [8]. An arbitrary ion spends t_a inside the source extracting field:

$$t_a = (2nd_a/v)(1 - n^2u - n^4u^2/2 + n^2w^2/2 - n^6u^3/2 + n^4uw^2/2) - 2n^2d_aw/v$$

t_b inside the accelerating source field:

$$t_b = 2nd_b/[v(n+1)][1 + nu + nu^2(n^2 + n + 1)/2 - nw^2/2 + nu^3(n^4 + n^3 + n^2 + n + 1)/2 - nuw^2(n^2 + n + 1)/2]$$

t_L along the whole field free space:

$$t_L = (L_f/v)(1 + u + 3u^2/2 - w^2/2 + 5u^3/2 - 3uw^2/2)$$

The meaning of the used symbol is $n = v/v_a$ with $n > 1$, $u = z_i/(2n^2d_a)$, $w = v_{z_i}/v$ where v_a and v are the reference ion velocities at the extracting field end and at the source exit grid, respectively.

The arbitrary ion remains during t_d inside the decelerating (at the entry) and reaccelerating (after reflection) stage of the mirror. t_d is twice the expression of t_b where d_b must be substituted by d_d and n by r. Here $r = v/v_d$ with $r > 1$ and v_d is the reference

ion longitudinal velocity at the mirror's intermediate grid. t_r is the time needed for reflection inside the mirror's second stage, twice the first term of t_a where n was substituted by r and d_a by d_r.

Finally, t_p the time spent inside the postaccelerating gap results by substituting the expression of t_b n by p and d_b by d_p. Now $p = v/v_p$, $p < 1$, with v_p the reference ion velocity after postacceleration. All these t_j time contributions have the form

$$t_j = a_{oj} + a_{uj}u + a_{wj}w + a_{uuj}u^2 + a_{wwj}w^2 + a_{uuuj}u^3 + a_{uwwj}uw^2$$

A certain ion arrives at the detector after t counted from the time origin:

$$t = t_i + a_o + a_u u + a_w w + a_{uu}u^2 + a_{ww}w^2 + a_{uuu}u^3 + a_{uww}uw^2$$

Here t_i is the time when the ion was produced, the "a" coefficients result by summing the "a_j" coefficients for the index j substituted by a, b, d, r, and p, respectively. $a_o = t_{\text{ref}}$ the flight time of the reference ion from source to detector

$$t_{\text{ref}} = \{2n[d_a + d_b/(1+n)] + L_f + 4r[d_r + d_d/(1+r)] + 2pd_p/(1+p)\}/v$$

To calculate the TOFMS resolution the ion packet length at the detector is needed. It results from the contributions of the time of ionization lasting, t_o (no delayed emissions are accounted for), due to the ion extraction from the depth of ionization region, between the origin and $u_o = z_{i_o}/(2n^2d_a)$, caused by the initial velocities distributed between 0 and $v_{z_{io}}$ if ions leave a surface (w varies between 0 and $w_o = v_{z_{io}}/v$), as well as from the detector time resolution t_D. If ions are created in gas phase, the initial velocities are distributed between $-v_{z_{io}}$ and $+v_{z_{io}}$ and the distribution width is doubled, thus accounting for the "turn-around" time. The packet length at the detector is $\Delta t = t_o + \delta t + t_D$ with the aberration term:

$$\delta t = |a_u|u_o + \lambda|a_w|w_o + |a_{uu}|u_o^2 + |a_{ww}|w_o^2 + |a_{uuu}|u_o^3 + |a_{uww}|u_o w_o^2$$

where λ is unity for ions from surfaces, 2 for ions from gas phase.

The a_w coefficient is $2n^2d_a/v$.

Another way to calculate the packet length is to use the formula [29]

$$\Delta t = (t_o^2 + \delta t^2 + t_D^2)^{1/2}$$

To resolve the ion packet of m mass ions from those of mass $m + \Delta m$ coming later, their arrival times must differ by more than the packet length. Approximately $t_{\text{ref}}\Delta m/2m \geq \Delta t$ and the resolution is $\Re = m/\Delta m = t_{\text{ref}}/2\Delta t$. Here the t_{ref} for the $m + \Delta m$ mass reference ion was considered to increase proportionally with $\Delta m/m$, compared with that of the m mass reference ion. In this resolution formula [30] we have to substitute the above-mentioned specific expressions for Δt.

3. Energy and position focusing

The homogeneous electrostatic field mirror, often called "reflectron," became, from its first-mentioned use [31], an usual means for ion energy focusing in time. At the ion source exit, the ions produced from various distances z_i in the extraction region will have, if we neglect their individual initial velocities, different energies U_i: $U_i = U(1+\delta) = U(1-2u)$ with the energy difference related to the reference ion $\delta = z_i/(n^2d_a)$. To ensure first order energy focusing in time a_u from the established flight time equality is to be canceled. When second order energy focusing is desired both a_u and a_{uu} must be canceled simultaneously. The remaining significant aberration is given by a_{uu} in the first, by a_{uuu} in the second case. Although second order energy focusing in time can be obtained only in two stage homogeneous electric field mirrors, for first order focusing a single stage mirror is preferred.

If single field sources are used (i.e. $d_b = 0$ and $n = 1$), neglecting the influence of the short postaccelerating gap $d_p = 0$, the second order energy focusing condition is fulfilled when

$$L_f = 2[2r^2d_d + (r^2-1)d_a]/(r^2-3)$$

$$E_d/E_r = (r-1)[(r-1)(r+2) + d_a/d_d(r+1)/r^2]/(r^2-3)$$

The total flight time is then

$$t_{\text{ref}} = (2/v)L_f(r^2-1)/r^2$$

while a third order aberration coefficient, that multiplies δ^3 forms a term to be included in the formula of Δt:

$$(r^2-1)L_f/(8v)$$

The minimal depth h of the mirror must be

$$h = d_d/[r(r^2-3)][r^3 - 2 - 2r^2/(r^2+1) + d_a/(r^2 d_d)]$$

formula to replace relation (70) of [8].

First order energy focusing in the single stage mirror is obtained if $L_f = 2(d_a + 2d_d)$, the total flight time is twice that spent by the ions in the field free space and the second order aberration coefficient is roughly $L_f/(4v)$.

The transversal dimension of the ion packet at the detector, if lenses are absent from the path, is $r_D = r_i + v_{r_i} t_{\text{ref}}$ where r_i and v_{r_i} are the radial initial extent and initial velocity, respectively.

The mass scale for the static field TOFMS results from the t_{ref} formula. If we add an offset constant c_0: $t = c_0 + c_1 m^{1/2}$ with c_1 also a constant.

4. Velocity focusing

The energy focusing in time, obtained with continuous voltages and electrostatic mirrors is in fact a hidden space focusing (compensating for the energy differences resulted from different start positions) as no focusing action is exerted upon the individual initial velocities as emphasized in [25].

In a source extracting field, constant in time, the first order term in velocity contributes to t_a by $2n^2 d_a v_{z_i}/v^2$ and cannot be compensated in this kind of field. The ion having higher initial velocity will be never caught by a slower one if both start simultaneously. The arrival time difference at the detector can be reduced however by higher accelerating voltages. The flight time differences induced by initial velocities may be corrected by an extracting field changing in time: established after some time interval T, counted from the ionization beginning, taken as time origin. As ionization lasts between 0.5 and 3 ns for nitrogen lasers [32,33], 80 ns for TEA CO_2 IR lasers [34], 0.8 ns for primary ion packets [35] the extraction field is connected usually after the ionization process ends. Therefore from the expression of Δt, t_o as independent term must be removed. After its formation, the ion with an initial velocity component v_{z_i}, will move freely until the extracting field is suddenly connected. If the ion was created at t_i, at the moment when the extracting field begins to act, its position will be $z_i = v_{z_i}(T - t_i)$. We substitute this in the terms t_s through t_p and keep, this time, also the other terms in v_{z_i} (in w). To detail the velocity focusing conditions we observe that in the rewritten form of t_s through t_p we have: $a_w = -na_o$, $a_{ww} = -a_u/2$, and $a_{uww} = a_{uu}$.

If we detail Δt as a series development in v_{z_i}, t_o we have $\Delta t = \delta t + t_D$ with

$$\delta t = |a_u|u_o + \lambda|b_v|v_o + |b_{vv}|v_o^2 + |b_{vt}|v_o t_o + |b_{vv}|v_o^2 + |b_{vvt}|v_o^2 t_o + |b_{vvv}|v_o^3$$

The new symbols are defined as

$$b_v = ka_u + a_w/v, \qquad b_{vt} = -a_u/(2n^2 d_a),$$

$$b_{vv} = k^2 a_{uu} + a_{ww}/v^2, \qquad b_{vvt} = -2a_{uu}k/(2n^2 d_a)$$

$$b_{vvv} = k(k^2 a_{uuu} + a_{uww}/v^2)$$

The higher order terms in u_o (in z_{io}, the thickness of the region of ion formation) were neglected.

The first order velocity focusing is obtained when b_v vanishes. This condition determines the time delay T as $k = T/2n^2 d_a$ or $T = -a_w/(va_u) = 2n^3 d_a t_{\text{ref}}/a_u$. Then the second order aberration coefficient is given by $b_{vv} = [a_{uu}(a_w/a_u)^2 + a_{ww}]v^2$. If second order velocity focusing is needed we have to cancel also b_{vv}. This happens when $a_{uu}a_w^2 = a_u^3/2$.

It is impossible to simultaneously obtain space

focusing and velocity focusing as the former needs $a_u = 0$ that makes T infinity. As stressed in [25] the first order velocity focusing condition depends on v (through t_{ref}), then on the ion mass, whereas the second order condition involves geometric parameters. The resolution deterioration on both sides of a selected mass can be easily followed by substituting the appropriate numerical values for v for the mass range of interest. Formulas for the simple cases of the single field source and of the single stage reflectrons are obtained by the substitutions $n = 1$, $d_b = 0$ and $r = 1$, $d_d = 0$.

As real world electronic units need some time interval to reach the final voltage after they are connected it is of practical interest to consider the influence of the extraction voltage increase time τ, on the ion motion. If the extracting field increases linearly from zero to its nominal value E_a (this increase will begin at T after the time origin), the integration of the equation of motion gives the space traveled by the ion during the field increase

$$z_{i\tau} = v_{z_i}\tau + qE_a\tau^2/(6m)$$

With the earlier notations z_i to be substituted in the expression of u, since the homogeneous constant field acts is

$$z_i = v_{z_i}(T - t_o + \tau) + v^2\tau^2/(12n^2d_a)$$

This is equivalent to the ion departure from a plane, having a mass dependent position, located at $v^2\tau^2/(12n^2d_a)$, closer to the exit grid, the time lag being $T + \tau$.

The time spent by ions inside the ionization chamber can be calculated analytically for a homogeneous electric field which approaches its final value following a time dependence of the form: $E_a[1 - \exp(-t/\tau)]$ [13], where τ is short compared with T and with the time spent by the ion inside the extraction space. The motion equation, by integration of the coordinate, gives

$$z = qE_a/m[t^2/2 - t\tau + \tau^2 - \tau^2\exp(-t/\tau)] + v_{z_i}t + z_i$$

From the condition $z = d_a$ when $t = t_a$ and neglecting the small terms in τ^2 we have

$$t_a = \tau + 2nd_a/v[-nw + (1 + n^2w^2 - 2n^2u - \tau vw/d_a)^{1/2}]$$

and taking again $\tau v/d_a$ as a first order small quantity the following third order expression results in:

$$t_a = \tau + 2nd_a/v(1 - nw - \tau vw/2d_a + n^2w^2/2 - n^2u - n^2\tau vuw/2d_a + n^2uw^2/2 - n^4u^2/2 - n^6u^3/2)$$

No matter what the ion nature is or the initial conditions are it has to additionally spend time τ in this space.

5. Quadratic potential mirrors

The most general form of the quadratic electrostatic potential [36] can be written as $\Phi(z) = k(z - a)^2 + C(x, y)$ where a is a constant and C is another one depending on the applied voltage. $C(x, y)$ may have different forms, but all must satisfy Laplace's equation. For plane symmetric distributions $C(x, y) = -k(x - b)^2/2 + dy + C_o$ with the particular case when the constants $b = d = 0$ the distribution may be produced by hyperbolic electrodes (Fig. 2).

If $C(x, y) = -k(x^2 + y^2)/4 + C_o$ the potential distribution can be produced by a stack of metallic rings. When $C(x,y) = -k(x^2 + y^2) + b\log[(x^2 + y^2)^{1/2}/d] + C_o$ conical and ring electrodes are necessary but a central electrode (prohibiting ion motion there) also must be included.

For all these distributions the ion motion along the z axis is described by [37]:

$$z - a = z_i\cos(\omega t) + v_{z_i}/\omega\sin(\omega t)$$

with $\omega^2 = qk/m$. If $a = z_i = 0$ ions leaving the $z = 0$ plane will return to this plane after reflexion no matter their initial velocity or direction is. It will happen after $t = \pi/\omega$ as the argument of sinus must

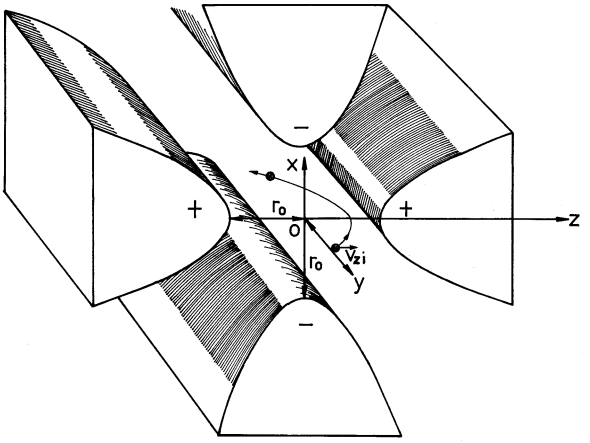

Fig. 2. Electrode structure able to create a two-dimensional quadratic potential.

be π to cancel the z coordinate. So t depends exclussively on the ion mass.

This kind of field have however two important inconveniences: the dramatic increase of the transversal packet dimensions to the detector and the absence of the field free paths from the ion circuit. The transversal expansion of the ion packet results from the ion x and y coordinates:

$$x = x_i \cosh(\omega t) + v_{x_i}/\omega \sinh(\omega t)$$

$$= 11.592x_i + 11.549v_{x_i}/\omega$$

$$y = y_i + v_{y_i}t = y_i + \pi/\omega v_{y_i}$$

If the field has an axially symmetric structure the radial ion motion is described by

$$r = r_i \cosh(\omega t/\sqrt{2}) + v_{r_i}\sqrt{2}/\omega \sinh(\omega t/\sqrt{2})$$

$$= r_i \cosh(\pi/\sqrt{2}) + v_{r_i}\sqrt{2}/\omega \sinh(\pi/\sqrt{2})$$

$$= 4.665r_i + 6.433v_{r_i}\sqrt{2}/\omega$$

The absence of the field free spaces makes it difficult to locate the ion source (or collision chamber) and the detector. The addition of field free spaces implies the loss of higher order focusing properties. However by appropriately choosing the constant a, first order velocity focusing can be restored [38]. The added field free space L_a is connected to a by

$$-a = [1 - (1 - L_a^2\omega^2/v^2)^{1/2}]/(L_a\omega/v^2)$$

The depth h where the reference ion penetrates inside the mirror is $h = v/\omega + a$ with $v = \omega(2U/qk)^{1/2}$.

A potential distribution was calculated for perfect energy focusing mirrors [39]. The mirror consists of a decelerating field gap, the potential inside the reflecting part being matched to the field free space of length L_f. An integral equation is solved with the help of a Laplace transformation and the ideal energy focusing potential is obtained in an implicit form:

$$z = (L_f + 2d_d)/\pi[\sqrt{\Phi/\Delta} - a \tan(\sqrt{\Phi/\Delta})] + \Phi/\Delta[1 - 2/\pi a \tan(\sqrt{\Phi/\Delta})]$$

Here d_d and Δ are the decelerating stage depth and the potential difference applied on it. Another field distribution created to ensure improved time focusing by electrostatic mirrors is the so called "curved field" [40–42]. A SIMION plot of such a potential indicates an arc of circle as a section by the Φz plane, whereas for homogeneous fields it is a straight line. This kind of field was used in tandem TOFMS to reduce the distance between the energy focuses of fragment ions of different mass.

Gridless mirrors feature transversal focusing properties and offer better sensitivity. Their design is based heavily on computer calculations. A recent design is described in [43].

6. Cylindrical electrostatic mirrors

Cylindrical electrostatic field reflectrons may be valuable alternatives to the classical homogeneous field mirrors. The constructive complication can offer as a reward, transversal focusing for instance. Single stage second order energy focusing by cylindrical mirrors would allow better sensitivity by eliminating the ion losses by collisions with the extra grid wires.

The simplest geometry of a cylindrical reflectron is given in Fig. 3 [44]. A cylindrically shaped inner grid is curved with r_o radius and grounded. Another concentric electrode is polarized to create the $1/r$ type field. The reference ion sent in the radial direction is

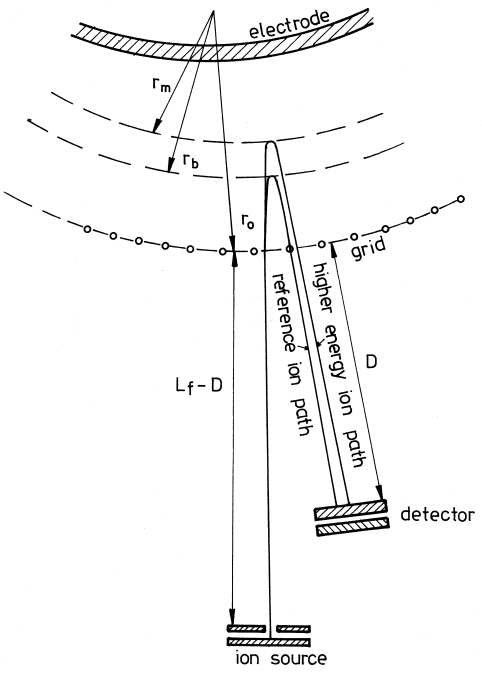

Fig. 3. Cross-section normal to the field symmetry axis through a cylindrical electrode reflectron.

supposed to stop at r_b (first we assume $r_b > r_o$). For an ion of higher energy $U_m = U(1 + \delta)$ the turning point is located deeper inside the field at r_m. The time spent inside the mirror can be calculated by

$$t = \pm \int_{r_0}^{r_m} dr/v(r)$$

$$= 2r_m[m \log(r_m/r_o)/(2q\Phi_m)]^{1/2} \int_0^{\sqrt{\log(r_m/r_o)}} \exp(-x^2)\, dx$$

After some developments:

$$t = \{4r_bI_c + 2a\delta(r_o + 2ar_bI_c) + a\delta^2[r_o(a^2 - 1/2) + 2r_ba^3I_c]\}/v$$

where

$$I_c = \int_0^a \exp(-x^2)\, dx, \qquad a^2 = \log(r_b/r_o)$$

By adding the contribution of the field free space the condition to cancel the term in δ can be prescribed. It determines the length of the field free space needed to obtain energy focusing at the detector: $L_f = 4a^2(r_o + 2ar_bI_c)$. In the general formula of the resolution t_{ref} must be substituted by: $t_{\text{ref}} = (4ar_bI_c + L_f)/v$. In this configuration $\Delta t = t_o + \delta t + t_D$ and we have to substitute for δt besides the initial velocity (or turn around term) the aberration due to δ^2:

$$\delta t = \lambda|a_w|w_o + |b_{\delta\delta}|\delta^2$$

The second order coefficient being

$$b_{\delta\delta} = [a^2r_o(a^2 - 1/2) + 2a^5r_bI_c + 3L_f/8]/v$$

A numerical exploration shows that there is no possibility to cancel both the coefficients in δ and δ^2 simultaneously in this case.

If $r_o > r_b$, i.e. when the convexity of the electrodes is oriented toward the source, first order energy focusing in time is achieved for the following field free space length:

$$L_f = 4b^2(r_o - 2br_bI_d), \qquad b^2 = -\log(r_b/r_o),$$

$$I_d = \int \exp(x^2)\, dx.$$

The total flight time for the reference ion is: $t_{\text{ref}} = (2br_bI_d + L_f/2)/v$. In the expression of δt we account, this time, for third order terms in δ. $\delta t = \lambda|a_w|w_o + |b_{\delta\delta}|\delta^2 + |b_{\delta\delta\delta}|\delta^3$ where the aberration coefficients are

$$b_{\delta\delta} = \{3L_f/8 + b^2[2b^3r_bI_d - r_b(b^2 + 1/2)]\}/v$$

$$b_{\delta\delta\delta} = \{-5L_f/16 + (b^2/3)[r_o(b^4 + b^2/2 + 3/4) - 2b^5r_bI_d]\}/v$$

Second order energy focusing in time is obtained for $r_b = 0.7013\ r_o$ and $L_f = 0.6188\ r_o$. Then the third order aberration in δ has the numerical coefficient $-0.0775r_o/v$. A two stage cylindrical field reflectron was constructed for Si_n, Si_nC, and Si_nO ion cluster studies [45]. The cylindric field ensures smaller trans-

versal distances, between points where different mass ions are focused in time, than for the homogeneous field reflectrons. The mirror was calculated to obtain second order energy focusing by canceling derivatives of the flight times written in an integral form. The curvature radii of the electrodes were of 1, 1.12, and 1.254 m the applied voltages 0, 4, and 7.4 kV, respectively. Resolutions of 4000 at FWHM were obtained routinely on aluminium cluster ions.

7. Tandem mirror systems

An efficient method to increase TOFMS resolution is to use a number of distinct cylindrically symmetric mirrors [46]. A specific geometry was tested and the resolution measured first without reflection, after 1 m flight (resolution 150), after one reflection and 3.5 m flight (550 resolution) and after 4.5 m (730). The main peak width was 60, 55, and again 55 ns, respectively.

With two electrostatic mirrors with plane symmetry, face to face, multiple reflections can be produced by properly selecting the source detector distance and the ion incidence angle to the mirror entry plane. Four parallel grids and two metallic sheets create two double stage mirrors, face to face. The ions injected obliquely performed a number of consecutive reflections before resulting in detection. A resolution of 3570 was obtained [47].

By switching two or three mirrors located face to face a prescribed number of reflections can be accomplished [46]. Two collinear axially symmetric mirrors are located between the ion source and the detector. At first, the two mirrors are at ground potential. The ions delivered in packets enter in the space between the two mirrors. The ion mass interval is selected by the delay when the mirrors are activated. Only ions located between the mirrors will be analyzed. The ions can be reflected an even number of times before admittance into the detector. A TOFMS with a MALDI ion source using this layout attained resolutions over 55 000 by using delayed ion extraction for velocity focusing [5]. The two 25 ring mirrors with two grids each were activated with switching times of 15 ns. To eliminate the too low response speed, the resistor divider was removed and mirrors operated as plain mirrors which do not compensate ion energy spread. Ions were accelerated by 10.5 kV whereas to the mirrors 13 kV were applied. The nitrogen laser delivered pulses of 3 ns FWHM in length. The ion source has an extracting gap of 1.18 cm and an accelerating gap of 1.1 cm. The mirror's depth is 3.5 cm, being separated by 81.6 cm. An even number of reflections were obtained with the molecular ion of substance P, of 1347 u the detection being accomplished after a time of flight of (number of cycles − 1) × 51.5 μs + the time needed to reach the detector in direct mode. For five cycles the flight time was 297 μs and the monoisotopic peak widths of 2.7 ns (55 000 resolution). The resolution increases linearly with the number of cycles whereas the peak width is almost constant. The peak height decreases after six reflections by 16 times. As the ions pass four times through grids for each reflection, the attenuation for six reflections is $T^{(6\times4)}$. The transparency of the grid T, results from the attenuation to be 89%, very close to the specified value.

Another arrangement uses three mirrors [46]. The ion source sends the ion packet through a grounded mirror under some incidence angle on a static mirror. It is reflected onto a third mirror which is activated in front of the detector after the mass interval was selected. Ions are reflected back to the static mirror which reflects them toward the source's mirror activated in the mean time. The reflection sequence can be repeated until the third mirror is grounded and the ions detected. A spectrometer located in a 700 mm long tube was used to demonstrate this principle on ions of 28 u and 500 eV. Moving once through the system the resolution was 260 and increased to 720 for the next step proportional to the ion path.

8. Hybrid quadrupole trap-electrostatic mirror instruments

Quadrupole ion traps are used to accumulate ions for a while, delivered next in short bursts for TOF analysis [48] (Fig. 4). The ion drawing out is performed by creating an extracting field inside the trap,

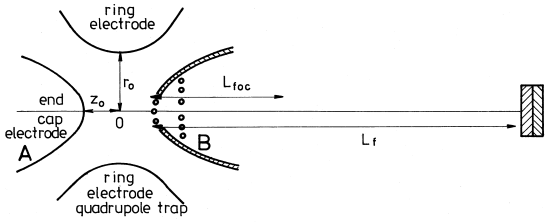

Fig. 4. Quadrupole trap-linear drift space time-of-flight analyzer hybrid system.

by altering the continuous potential applied to one endcap electrode whereas the radio frequency signal is supressed or reduced to an insignificant value [49]. The quadrupole trap can itself work in an extracting regime [50] or the trap can be associated with an Einzel lens [51]. The extraction process from the ion trap creates a longitudinal (time) focus, its position being largely determined by the applied potentials and can be located by simulation. From the intermediate focus thus formed an electrostatic mirror produces an energy in time focus on the detector.

A quadrupole ion trap having $r_o = z_o\sqrt{2} = 10$ mm was fitted through an Einzel lens to a two stage gridless mirror [50]. A second order space focus is obtained at 300 mm from the laser ionization point (trap middle), result obtained by SIMION [52] simulation. To extract ions a dc potential of 1.5 kV during accumulation is reduced to 1 kV on the extracting endcap whereas an ac voltage on the ring electrode is reduced from 1.5 to 0.36 kV. The second order space focus is used for ion photodissociation by a second laser. The mirror's first stage is set to 0.8 kV. On the 78 u benzene ion the resolution was 1120 FWHM. Storage times extending to 10 s were used for a mass range of the trapped ions extending until 1600 u. By variation of the mirror's end plate potential ion energies were measured (the ions just allowed to pass having the energy equal to the applied potential multiplied by their charge). The ion pellet formation from externally injected particles, as well as the role of parameters as initial rf voltage phase and ion trapping times, were studied in detail by simulation for this instrument [51].

A parabolic potential electrostatic mirror was connected to a modified commercial detector trap [53]. The extraction regimes were simulated. The ions enter the parabolic reflectron through a central hole, in the multichannel plate.

9. Homogeneous electric field single and two field sources followed by drift space

The space (position) focusing in time in a linear TOFMS happens in fact in the second half of an energy focusing device as an electrostatic mirror. For simplicity, we assume the field free space traveled before and after reflection as being of equal lengths, the entry and exit of ion packets normal to the mirror boundary.

The ions of different energies sent into the mirror will stop at various depths inside the retarding field. If they started simultaneously from the end of the field free space, they will stop simultaneously inside the mirror. The re-acceleration process simultaneously forms an energy focus of the original packet at the end of the second field free space. At the same point a space focus will be achieved for the ions which stopped inside the decelerating field. This kind of space focusing was used in a TOFMS mirror where photodissociations are induced at the ion trajectories turning points [54,55]. Usually in the two stage mirror second order energy focusing TOFMS the decelerating field is much more intense than the reflecting one. Similarly, in the two field source of a linear TOFMS, the extracting field is weaker than the final accelerating one.

The time lapses spent by ions in the linear TOFMS are given by the expressions of t_a, t_b, t_L, t_p written for the homogeneous electric field reflectron. We neglect the short postacceleration trajectory position. The first order space focus, when $a_u = 0$ in the total flight time accounting for the above trajectory section is located at $L_f = 2n^2[d_a n - d_b/(1 + n)]$. The second order space focus is obtained if simultaneously L_f satisfies also the condition: $L_f = 2n^2/3[d_a n^3 - d_b(n^2 + n + 1)/(n + 1)]$. In the second order space focusing case the range of parameters is somewhat restricted [56]. A geometric condition can be written as [57]

$$d_a = (L_f - 2d_b)\{L_f[(L_f - 2d_b)/(3L_f)]^{3/2} + d_b\}/[2(L_f + d_b)]$$

In the resolution formula the reference ion total flight time is mainly due to the field free space and the terms representing the flight inside the ion source are often only a small correction:

$$t_{\text{ref}} = \{L_f + 2n[d_a + d_b/(n+1)]\}/v$$

The coefficients involved in δt are those given in the general formula but the "*a*" coefficients are obtained now only by summing for the t_a, t_b, t_L, and t_p flight time contributions.

A single stage reflectron focuses in time ions of different energies after a field free space four times the mirror depth [58]. The single field source TOFMS is half the above-mentioned value: space focusing ions at the end of a field free space twice the accelerating space depth (used in real instruments only to create an intermediate focus).

10. Velocity focusing

Time lag focusing consists in the delayed ion extraction, leaving ions to move in a field free environment after their formation. Initially it was used for ions created from gas phase molecules [1]. Delayed extraction [10–12] became the most efficient procedure to aleviate defocusing effects for MALDI born ions.

The velocity focusing conditions derived for the reflectron simplify somewhat in detail by the absence of the terms originating from t_d and t_τ. The time delay formula remains the same in terms of n, d_a, and a_u.

As in the TOFMS including mirrors, the velocity focusing is achieved only for a mass that determines the time delay when the extracting field is applied. The possibility to extend velocity focusing on a range of mass values was explored in [59] for a single field source-drift space TOFMS. The extracting potential should be adjusted in time in such a way that starting from a minimal mass m_{min} correctly velocity focused, the other mass ions receive a different energy supplement by an extracting field adjusted in time. This procedure acts until a mass m_{max} is reached. Numerical calculations include the solution of a differential equation to find the appropriate shape for the applied extracting voltage. In realistic MALDI conditions resolutions of up to 4480 result on a mass range of $m_{\text{max}}/m_{\text{min}}$ of 10. The procedure was extended and modified to two field source linear TOFMS [60], starting the correction from m_{max} backwards. Resolution enhancements of seven times and more were predicted for adequate parameter choice.

11. Postsource focusing

Postsource focusing can be used in linear as well as in reflectron TOFMS. An additional grid must be placed somewhere at d_{ps}, downwards from the ion source exit on the ion packets' path. At a given time T, measured since the ionization beginning, a homogeneous electric field, E_{ps} is applied suddenly between the last source grid, at ground and the additional grid [61]. Only ions being inside the postsource accelerating interval, after the field connection undergo extra focusing. The ions deeper inside the accelerating interval will be less accelerated than those having a longer distance to travel inside this additional field. Ions coming later are those with a higher mass, all of them are generated later in the ion source. That means that the delayed ions will be more accelerated and they eventually will catch up those being closer to the detector at that time. A bunching of the ion packets and initial velocity focusing can be obtained simultaneously. Ions steping in the postsource accelerating space after the field was established receive all the same acceleration as they would if they were emitted from a triple field ion source. How the created PSF potential effects ion paths on the other grid side is of little interest because this field is weak enough (even if its action should be cumulative until the detector).

The basic geometric parameters that define a TOFMS with postsource focusing are shown on Fig. 5. Some ion formed at t_i after the time origin will step inside the additional acceleration space after the time

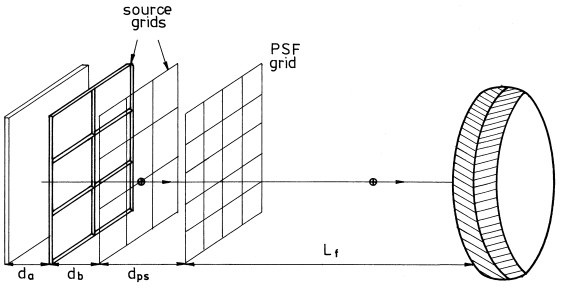

Fig. 5. Definition of the electric toroidal deflector geometric parameters, main path in a plane normal to the distribution symmetry axis.

spent inside the source where constant fields are applied. If the PSF field is connected later the ion travels still unperturbed some distance inside the postsource accelerating space. It depends on its velocity (and on its mass) how long it has to move inside the applied accelerating PSF field.

In a first order approximation the time when an ion arrives to the detector is

$$t_{\text{tot}} = T + 2d_{\text{ps}}U/(vqE_{\text{ps}}d_{\text{ps}}[f(1 + k_1t_i - k_2v_{z_i}) - 1] + L_d/(vf)(1 - k_1t_i + k_2v_{z_i})$$

where $f^2 = 2qE_{\text{ps}}D_p/U + 1$, $k_1 = (1 - 1/f^2)v/(2D_p)$, $k^2 = d_an^2(1 - 1/f^2)/(D_pv)$, and $D_p = d_{\text{ps}} + 2n[d_a + d_b/(1 + n)]$. Focusing of v_{z_i} components, simultaneously with bunching (t_o length packet compression) happens when $L_d = 2Uf^2d_{\text{ps}}/(qE_{\text{ps}}d_{\text{ps}})$. As f depends on D_p and this last on v, the above-mentioned condition reveals a mass dependence. Only ions of a given mass will be exactly focused at first order. The focusing action extends over some mass interval, but correct first order focusing is obtained only for a selected mass.

The mass range where ion focusing is modified by the PSF field is

$$UT^2/\{2n^2[d_a + d_b/(1 + n) + d_{\text{ps}}]^2\} < m < UT^2/\{2n^2[d_a + d_b/(1 + n)]^2\}$$

The mass scale function is cumbersome but straightforward to derive from the total flight time of the reference ion:

$$t_{\text{ref}} = c_0 + m^{1/2}[c_1(1 - c_2m^{-1/2})^{1/2} + c_3 + c_4/(1 - c_2m^{-1/2})^{1/2}]$$

The mass scale calibration is a more difficult task here than for constant field TOFMS because an increased number of c_i constants must be determined.

A somewhat simpler mass dependence was successfully used in experimental work [62]. The melitin MH^+ ion mass at 2845.75 Da was measured with an average error (rms) of 0.09 Da that means less than 40 ppm. The calibration was done by using the dependence form: $t = c_0 + c_1m^{1/4} + c_2m^{1/2} + c_3m^{3/4}$.

Improved resolution and sensitivity were obtained on a linear TOFMS having the following basic geometric parameters [17]: $d_a = 10$ mm, $d_b = 5$ mm, $d_{\text{ps}} = 90$ mm, and $L_d = 1899$ mm. Sensitivity improvements resulted from the use of an intermediate electrode without a grid used as a lens, located before the grounded source electrode, polarized at 19.77 kV as the extracting electrode (repeller at 20 kV). The mass accuracy determination was improved by using single laser shot mass spectra instead to average them. Thus the broadening due to shot to shot jitter was eliminated. It was possible to obtain resolutions of 8600 on the molecular ion peak of insulin at 3495.62 ± 0.04 Da measured with 60 ppm error.

Looking for other reasons of resolution limitations, the effect of the PSF applied pulse were simulated with the SIMION program. The linear rise of the PSF field to its nominal value in less than 500 ns increases the ion packet length by less than one ns at FWHM, while the applied voltage increases from 0 to 2.9 kV in 30 ns on the first PSF region electrode. The 3% linear decrease of the PSF nominal applied voltage in 10 μs has no visible effect on the simulated resolution [62].

12. Inhomogeneous accelerating electric fields

The parabolic potential distribution features perfect space focusing. If the ions start without initial velocity from the initial coordinate z_i they will arrive to the $z = 0$ plane after a time depending only on

their mass. By substituting $t = \pi/(2\omega)$ into the z motion equation, established before, the final coordinate results to be $z = 0$ [63]. The focusing properties of this kind of field were embodied in a 5000 resolution instrument for electrospray ions and the aspects concerning both space and energy focusing discussed [64].

A potential distribution ensuring perfect space focusing properties was calculated [65]. The ion accelerated inside this distribution passes by an additional accelerating gap d_b, through the potential difference Δ, before traveling over a field free space. The ideal potential was obtained as solution of an integral equation after Laplace transformation. It was given in an implicite form

$$z = 2/\pi(L_t + d_b)[(\Phi/\Delta)^{1/2} - a\,\tan(\Phi/\Delta)^{1/2}] + \Phi/\Delta[1 - 2/\pi a\,\tan(\Phi/\Delta)^{1/2}]$$

13. Hybrid quadrupole trap–TOF analyzer systems

Quadrupole traps were connected to linear TOFMS. To extract ions accumulated in the trap the field was established between one endcap and an external grid [66–68]. The ions are focused directly on the detector after flying over a field free space of appropriate length.

Ions produced by electrospray were injected through a sampling skimmer and plate stack in a quadrupole trap. The ions extracted through a 3 mm diameter opening in the endcap at 5 mm from the accelerating grid before being left to fly free on 0.9 m. The ion extraction happens during the 30 μs when the endcap is polarized at -500 V. The trapping time was typically 100 ms followed by a 1.2 μs rf voltage decay. Mass resolution of 920 FWHM was obtained for the cytochrome c, $[M + 16H]^{16+}$ peak, in the range 600–1200 for equine apomyglobin, high mass to charge ratios allowing the detection of 150 000 Da antibodies.

Perfect velocity focusing may be obtained for ions emitted from the tip of a quadrupole endcap electrode [69] (see Fig. 4). An aperture in the opposite endcap must allow ion motion over a field free path. The ion acceleration must be obtained by rectangular voltage pulses applied to the quadrupole trap electrodes, delayed with respect to the ionization process. If a pulse of T_c length is applied T seconds after an ionization-detection cycle beginning, perfect velocity focusing happens after a free flight path on $L_f = z_0/[\omega T\,\sin(\omega T_c) - \cos(\omega T_c)]$ dependent upon the ion mass through ω. In the general resolution formula we have to put

$$t_{\mathrm{ref}} = L_f/z_0[\sin(\omega T_c)/\omega + T(\omega T_c/\sin\,\omega T_c + \cos(\omega T_c)]$$

$$\Delta t = t_D + \{L_f\sigma/(1 + \sigma) + v_0[L_f t_0/z_0 + \sigma/\omega\,\sin(\omega T_c)]\}/[z_0\omega\,\sin(\omega T_c)]$$

The first order term in t_0 is absent, if $T > t_0$. The symbol $\sigma = (\delta r/2z_0)^2$ was introduced to account for ions emitted from points located inside a circle of δr radius on the endcap electrode tip.

For $z_0 = 2$ cm, $L_f = 1$ m, $t_0 = 0.8$ ns, $\delta r = 15$ μm, pulse height of 30 kV and initial energies spreaded over 30 eV, for 500 000 u ions the perfect velocity focusing conditions being satisfied, a resolution of about 220 000 is calculated. To ensure such high mass ion detection, postacceleration would be needed. Pulses of $T_c = 2.94$ μs should be applied since $T = 11$ μs.

14. Electrostatic deflectors

Multiple electrostatic sectors can be combined in configurations with multiple symmetries [70]. Four sectors can already ensure radial x, α, δ, yy, $y\beta$ time focusing simultaneously with transversal α, β, and δ focusing [71]. The used symbols are: x ion position projection distance to the main path in the deflection plane, y its distance to the deflection plane, α angle of the ion velocity projection on the deflection plane with the main path, and β with the median plane.

An instrument from four identical cells embodied this concept. Each cell contains a toroidal deflector (Fig. 6) of $\Phi_e = 269°$, field index $c = r_e/R_a =$

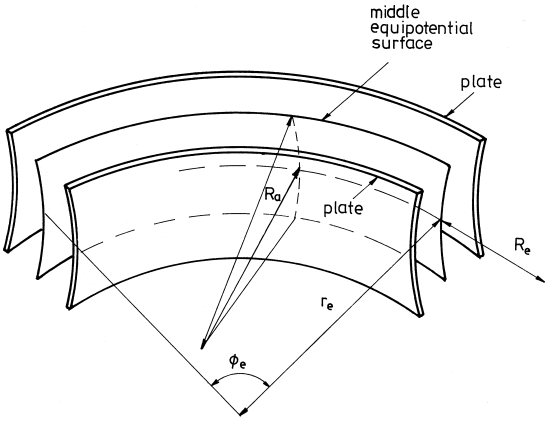

Fig. 6. Quarter of the symmetric structure of the closed orbit high resolution time-of-flight mass spectrometer.

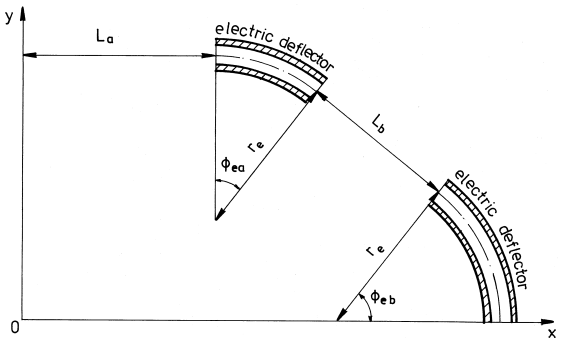

Fig. 7. Postsource focusing grid location between ion source and detector.

0.015, main path radius $r_e = 5$ cm (R_a = equipotential surface axial curvature radius at the main path), located between two field free spaces $L_1 = 11.9$ cm and $L_2 = 15.6$ cm, respectively. Assuming an equal radial and axial beam aperture of $\pm 5 \times 10^{-3}$ as well as a relative energy spread of the same magnitude, resolutions of 12 000, 23 500, and 33 400 were calculated after one, two and three complete turns. The aberrations were calculated by the third order program TRIO TOF [29].

Recently a six electric field deflector TOFMS was built to allow mass dispersion increase by multiple ion turns inside an ovale structure [72]. Once ions are admitted in the orbit they can accomplish as many turns as are acceptable from the point of view of the intensity losses. The structure has multiple symmetry properties. We can consider the system as constructed from four cells (Fig. 7), each 104.4° deflector being shared by two neighbor cells, symmetrically cut by a symmetry plane in two equal halves. The two assemblies of three condensers are symmetric with respect to the middle point O. This multiple symmetry ensures the cancellation of flight time aberrations in x, α, δ, $\alpha\delta$, $\beta\beta$ and offering transversal angular focusing in α, energy focusing in δ and practically also in β, as the irespective coefficient is very small. Aberrations were calculated accounting for third order contributions to the detected ion packet length. The following components were included: those in x, α, δ, α^2, $\alpha\delta$, δ^2, y^2, $y\beta$, β^2, α^3, $\alpha^2\delta$, $\alpha\delta^2$, δ^3, αy^2, $\alpha y\beta$, $\alpha\beta^2$, δy^2, $\delta y\beta$, $\delta\beta^2$.

The parameters defining each cell are $L_a = 0.593$ m, $L_b = 0.483$ m, $r_e = 0.5$ m $\Phi_{ea} = 37.8°$, $\Phi_{eb} = 90°–37.8°$, and $c = 0.293$.

In these calculations the transfer matrix elements of the main field of the sectors [73] and the more recently derived matrix elements for the fringing fields [29] were included. The elements of the time row are written as: (t/ijk) where i, j, and k are the already enumerated ion motion caracterizing quantities.

For the entry boundary they are

$$(t/t) = 1, \qquad (t/\alpha) = -2I_{1a}r_e/v \; (t/xx) = 3I_{4a}/(r_e v)$$

$$(t/xxx) = 1/(6r_e R_e v) \qquad (t/xx\alpha) = 1/(r_e v)$$

$$(t/xyy) = -1/(2r_e R_e v)$$

The following integrals are to be calculated over the electric field distributions at the deflector entry boundary:

$$I_{ta} = \int\int E/E_0) \; d\eta \; d\eta - \eta_b^2/2$$

$$I_{4a} = \int (E/E_0)^2 \; d\eta - \eta_b$$

with η a coordinate normal to the entry boundary and R_e the effective boundary curvature radius. The integrals are taken between a point "a" where the fringing

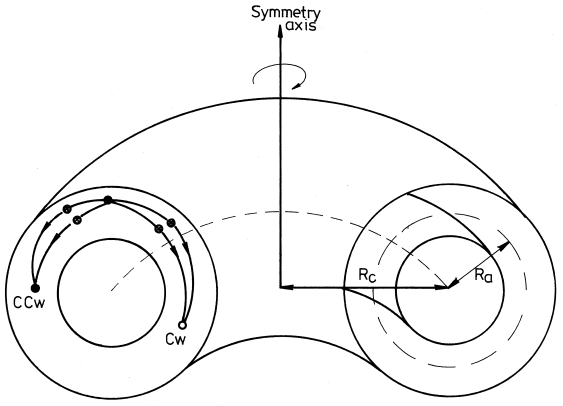

Fig. 8. Ion path in a plane containing the toroidal condenser symmetry axis of the poloidal deflector.

field E becomes negligible and a point "b" where the radial electric field E practically is identical with that in the main field E_0. For the exit boundary the time determining transfer matrix elements have all the same form, but (t/α) and $(t/xx\alpha)$ change their sign. For the exit boundary elements the irespective R_e value and electric field distribution (to calculate integrals) must be used.

15. Poloidal deflectors

Poloidal deflectors are prefered for space applications and as electron analyzers because of their wide 360° viewing angle [74,75]. A toroidal condenser becomes a poloidal deflector if reference particles are so directed that they move in a section of the condenser that contains the rotation axis (Fig. 8). The focusing properties of the poloidal deflectors were hard to explore because of the field and therefore the ion trajectories must be calculated numerically only. The transversal focusing properties were studied for such a deflector [74]. The focusing properties, including those that were time dependent, were given in a matrix form, as used in an equatorial plane description. A remarkable property is the dependence of the transfer matrix elements of the sense of motion: clockwise or counterclockwise. As an example, the time transfer parameters of an angle focusing poloidal analyzer having the first field free space of 5 mm, the second of 30 mm, equatorial curvature radius, denoted now by $R_c = 50$ mm, axial curvature radius 180 mm, respectively are given. The focusing angles were of 83.06° for clockwise motion and 101.38° for counterclockwise sense, the starting angle being −90° for both. The flight time elements were calculated to be $(t/x) = 1.17R_a/v$ and $0.97R_a/v$, respectively, $(t/\alpha) = 1.49R_a/v$ and $1.98R_a/v$; $(t/\Delta m/m) = 1.07R_a/v$ and $1.23R_a/v$ whereas $(t/\delta) = -0.28R_a/v$ and $0.13R_a/v$.

To ease calculations an analytic expression of the poloidal electrostatic potential was derived in a series of small involved quantities [76]. This allowed easy access to the second order matrix elements and to the calculation of the aberrations. A two poloidal deflector system ensuring simultaneous transversal angles and energy focusing concomitantly with energy focusing in time was calculated.

Two "nested" poloidal condenser geometries (one poloidal condenser inside the another) were studied to obtain simultaneously transversal angular focusing in the radial, parallel to point azimuthal focusing, with no lateral energy dispersion and with energy focusing in time [77].

The lack of transparency of the motion equations to be solved only numerically hinders the complete and general description of the ion optical properties of the poloidal deflectors.

16. Orthogonal injection and orthogonal extraction

To reduce the velocity distribution width along the extracting-accelerating direction the orthogonal ion injection is used [78].

The processes preceding the ion filling step direct the initial ion velocities mainly at right angles to the extracting field directions. The velocities along this field are small but the region of packet creation is deep enough, of the order of 2–3 mm in [79,80] to need space focusing. Additionally, to prohibit ion leakage during the filling period, a potential $\Phi = E_b(d_{gr}/2\pi)\ \log(d_{gr}/2\pi r_{gr})$ must be applied to the

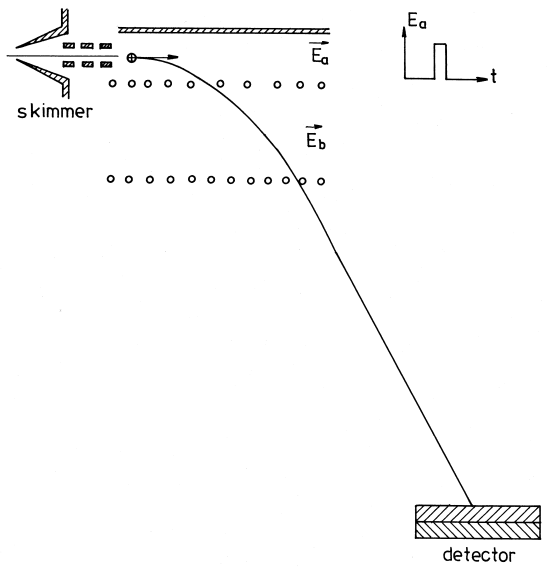

Fig. 9. Principle of the orthogonal extraction excluding the harmful effects of adjusting condensers.

filling space exit grid. The grid wires are of r_{gr} radius, located d_{rg} apart [81].

The analyte ions during extraction space filling have almost identical velocities. After extraction the ions keep their drift velocities v_{y_i} along the axis perpendicular to the accelerating field (Fig. 9): $v_{y_i} =$ const. They will reach the detector plane after $t_{tot} = L_{eff}/(2U/m)^{1/2}$. They will come to that plane shifted by $D_y =$ const $m^{1/2}$. Therefore a very limited mass range will be detected and most of the ions are missing from the detector area if this was placed in direct view from the source. As a simple practice, plane deflectors were used to redirect the ions on the detector from the mass range of interest. The use of the plane deflectors induces, according to [81], an ion packet curving effect, thus a flight time error of length δt_{def}:

$$\delta t_{def} = L_{eff}U/(qE_{df}L_{df})$$

where E_{df} is the deflector field intensity, L_{df} its effective length. The fringing fields of these deflectors impart different velocity components to the ions of the packet, increasing in fact the final temporal length.

The ion packet lengthening due to the packet deflection was eliminated by the new TOFMS design of Guilhaus and co-workers [82,83], called orthogonal extraction. In this design ions are extracted normally, the formed ion packet being left to fly unharmed. The detector, and the mirror if present, are displaced by design to allow the collection of the ions of the mass range of interest.

17. Double electric condensers

Electric plane deflecting condensers were used to chop packets from continuous ion beams [84]. Two deflectors operated together form ion gates that are able to select izotopomers for further analysis i.e. to perform tandem mass spectrometry [85,86]. Such deflectors can be constructed from simple plates or by assembling many metalic ribbons. Two neighboring ribbons are connected to opposite potentials. Devices constructed from interleaved deflection strips preserve low capacitance and the applied voltage pulses are close to the ideal rectangular shape. A double deflector made of two batches of 20 parallel nickel-chromium sheets of 1.27 × 15 mm, located 1 mm apart was used to select isotopomers from MALDI created ion packets [87]. The selection capability of the device was illustrated by its resolution of about 5200. Earlier simpler devices constructed from two condensers allowed resolutions of 300 to be attained without optimisation [88]. The resolution of a double deflector assembly can be derived easily assuming the deflecting fields to be homogeneous and accounting for the fringing fields by the effective boundary position and thus by its effective length. It is often assumed that the electric field extends with a gap outside the physical limit of the plate.

The ion packets are coming from the ion source located at L_g from the first condenser's effective limit (Fig. 10). The field inside the first condenser begins to decrease at T_p after the packet front left the source. Therefore an ion of appropriate velocity v is submitted to the entire electric field $-E$ during t_e. The electric field of the first condenser vanishes during τ. T, later in the field of the second condenser, also increases (linearly) during τ. So the ion was submitted

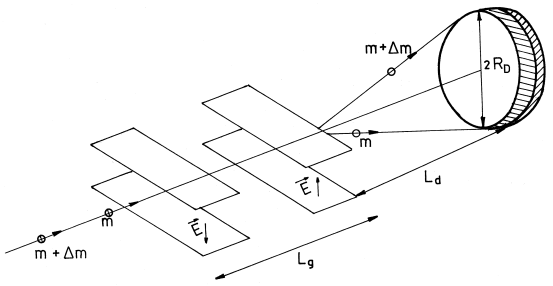

Fig. 10. Separation of different mass ion packets by time dependent deviation in a two tandem plane condenser assembly.

to the field E during t_f, when it leaves the second condenser. It arrives to the detector of radius R_D (or to a limiting slit) after a flight over a field free space of length L_D. The ion position is given as quadratic time dependence inside the static field and as cubic in the linearly increasing (or decreasing) field. The position of the ion at the detector or at the limiting slit, in the plane of deviation is a function of the mass:

$$y = y_i + v_{y_i}(t_e + 2\tau + T + t_f + L_D/v) - qE/m[t_e^2/2 + 2t_e\tau + \tau^2/2 + Tt_e + T\tau/2 + t_e t_f - t_f^2/2 - L_D/v(t_f - t_e)]$$

Roughly, y_i and v_{y_i} can be neglected. An ion having higher mass $m + \Delta m_2$ having the velocity $v(1 - \Delta m/m)$ will be less deviated than that with v. To have the ions of mass m resolved from those of $m(1 + \Delta m/m)$ the axes of the two successive packets must be at a distance of at least $2R_D$ at the detector plane. From the difference of the deviations of the two mass ions we get the resolution

$$m/\Delta m = \{(L_d + L_g + L_s)(T + 2T_p) - 2\tau L_s + v[\tau(\tau + 4T_p + T) - 2T_p(T + T_p) - T^2]\}qE/(4mvR_D)$$

If we put the deviation $y = R_D$, we neglect L_g with respect to L_s and L_d, the terms in τ and approximate T_p by L_g/v we obtain $m/\Delta m = qEL_gL_d/(2R_DU)$ relation given in [87].

18. Conclusions

The already well established TOFMS configurations are the subject of further refinements and progress by the continuous technical development of lasers delivering shorter pulses, detectors with better time resolution, by higher accuracy in pulse shape generation, and in keeping constant the repetition rate.

The TOFMS resolution improvements should result from the reduction of the ion packet initial distributions in space and velocity. It would be of interest to explore how much these distributions can be reduced by cooling ions in quadrupole traps before TOF analysis, without limiting by the mass range. The cylindrical and spherical electrode mirrors could disclose higher order energy focusing in time associated with transversal focusing, to keep sensitivity high. The increase of the mass dispersion for TOFMS is a sure way to improve mass resolution. For the close orbit TOFMS this can be done by watching to minimize ion losses in orbit. Multiple reflection by opposite mirrors, preferably without grids, shaped to keep longitudinal and transversal ion packet dimensions unchanged are another, proved already to be a fruitful solution.

A mass dispersion of doubling results by using constant momentum ion packets instead of constant energy ions. The possibility to obtain mass dispersion increase by time dependent voltages applied on the mirror electrodes is a topic also to be explored.

References

[1] W.C. Wiley, I.H. McLaren, Rev. Sci. Instrum. 26 (1955) 1150.
[2] U. Bahr, U. Roehling, C. Lautz, K. Strupat, M. Schueerenberg, F. Hillenkamp, Int. J. Mass Spectrom. Ion Processes 153 (199) 9.
[3] M. Karas, J. Mass Spectrom. 33 (1997) 1.
[4] T. Bergmann, T.P. Martin, H. Schaber, Rev. Sci. Instrum. 60 (1989) 792.
[5] C.K.G. Piyadasa, P. Hakansson, T.R. Ariyaratne, Rapid Commun. Mass Spectrom. 13 (1999) 620.
[6] H. Wollnik, private communication.
[7] R. Stein, Int. J. Mass Spectrom. Ion Processes 131 (1994) 29.
[8] D. Ioanoviciu, Int. J. Mass Spectrom. Ion Processes 131 (1994) 43.

[9] S.M. Colby, T.B. King, J.P. Reilly, Rapid Commun. Mass Spectrom. 8 (1994) 865.
[10] R.S. Brown, J.J. Lennon, Anal. Chem. 67 (1995) 199.
[11] R.M. Whittal, L. Li, Anal. Chem. 67 (1995) 1950.
[12] T.B. King, S.M. Colby, J.P. Reilly, Int. J. Mass Spectrom. Ion Processes 145 (1995) L1.
[13] S.M. Colby, J.P. Reilly, Anal. Chem. 68 (1996) 1419.
[14] Y. Zhu, L. He, J.R. Srinivasan, D.M. Lubman, Rapid Commun. Mass Spectrom. 11 (1997) 987.
[15] R.M. Whittal, L.M. Russon, S.R. Weinberger, L. Li, Anal. Chem. 69 (1997) 2147.
[16] R.M. Whittal, D.C. Schriemer, L. Li, Anal. Chem. 69 (1997) 2734.
[17] G.R. Kinsel, J.M. Grundwuermer, J. Grotemeyer, J. Am. Soc. Mass Spectrom. 4 (1993) 2.
[18] A. Benninghoven, Angew. Chem. Int. Ed. Eng. 33 (1994) 1023.
[19] A. Benninghoven, B. Hagenhoff, E. Niehuis, Anal. Chem. 65 (1993) 630A.
[20] A. Verentchikov, W. Ens, J. Martens, K.G. Standing, Proceedings of the 40th ASMS Conference on Mass Spectrom Allied Topics, Washington DC, 1992 p. 360.
[21] R.C. Beavis, B.T. Chait, Chem. Phys. Lett. 11 (1991) 479.
[22] Y. Pan, R.J. Cotter, Org. Mass Spectrom. 27 (1992) 3.
[23] M. Schuerenberg, T. Schula, K. Dreisewerd, F. Hillenkamp, Rapid Commun. Mass Spectrom. 10 (1996) 1873.
[24] A.N. Verentchikov, W. Ens, K.G. Standing, Anal. Chem. 66 (1994) 126.
[25] M. Vestal, P. Juhasz, J. Am. Soc. Mass Spectrom. 9 (1998) 892.
[26] U.N. Andersen, A.W. Coburn, A.A. Makarov, E.N. Raptakis, D.J. Reynolds, P.J. Derrick, S.C. Davis, A.D. Hoffman, S. Thomson, Rev. Sci. Instrum. 69 (1998) 1650.
[27] D. Ioanoviciu, G.E. Yefchak, C.G. Enke, Int. J. Mass Spectrom. Ion Processes 94 (1989) 281.
[28] D. Ioanoviciu, Rapid Commun. Mass Spectrom. 7 (1993) 1095.
[29] T. Sakurai, T. Matsuo, J. Mass Spectrom. Soc. Jpn. 46 (1998) 437.
[30] H. Wollnik, Int. J. Mass Spectrom. Ion Processes 131 (1994) 387.
[31] B.A. Mamyrin, V.I. Karataev, D.V. Shmikk, V.A. Zagulin, Sov. Phys. JETP 37 (1973) 45.
[32] K. Dreisewerd, M. Scuerenberg, M. Karas, F. Hillenkamp, Int. J. Mass Spectrom. Ion Processes 141 (1995) 127.
[33] K. Dresewerd, M. Schii, M. Karas, F. Hillenkamp, Int. J. Mass Spectrom. Ion Processes 154 (1996) 171.
[34] Ch. Menzel, S. Berkenkamp, F. Hillenkamp, Rapid Commun. Mass Spectrom. 13 (1999) 2.
[35] E. Niehuis, T. Heller, U. Juergens, A. Benninghoven, J. Vac. Sci. Technol. A 7 (1989) 1823.
[36] V.P. Ivanov, A.A. Makarov, A.A. Sysoev, Proceedings of the IVth International Seminar of Scientific Space Instrumentation, V.M. Balebanov (Ed.), Moscow, 1990, Vol. 2, p. 65.
[37] A.L. Rockwood, Proceedings of the 34th ASMS Conference on Mass Spectrometry of Allied Topics, Cincinnati, Ohio 1986, p. 173.
[38] A.A. Makarov, E.N. Raptakis, P.J. Derrick, Int. J. Mass Spectrom. Ion Processes 146/147 (1995) 165.
[39] C.A. Flory, R.C. Taber, G.E. Yefchak, Int. J. Mass Spectrom. Ion Processes 152 (1996) 177.
[40] T.J. Cornish, R.J. Cotter, Rapid Commun. Mass Spectrom. 7 (1993) 1037.
[41] T.J. Cornish, R.J. Cotter, Rapid Commun. Mass Spectrom. 8 (1994) 781.
[42] M.M. Cordero, T.J. Cornish, R.J. Cotter, Rapid Commun. Mass Spectrom. 9 (1995) 135.
[43] J. Zeng, M. Karas, F. Hillenkamp, Proceedings of the 43rd ASMS Conference on Mass Spectrometry of Allied Topics, Atlanta GA, Santa Fe, 1995 p. 1205.
[44] D. Ioanoviciu, R. Stein, A. Ioanoviciu, unpublished results.
[45] J.L. Vialle, B. Baguenard, A. Bourgey, E. Cottancin, J. Lerme, B. Palpant, M. Pellarin, F. Valadier, M. Broyer, Rev. Sci. Instrum. 68 (1997) 2312.
[46] H. Wollnik, M. Przewloka, Int. J. Mass Spectrom. Ion Processes 96 (1990) 267.
[47] C-S. Su, Int. J. Mass Spectrom. Ion Processes 88 (1989) 21.
[48] B.M. Chien, S.M. Michael, D.M. Lubman, Int. J. Mass Spectrom. Ion Processes 131 (1994) 149.
[49] U. Wilhelm, K.P. Aicher, J. Grotemeyer, Int. J. Mass Spectrom. Ion Processes 152 (1996) 111.
[50] K.P. Aicher, M. Mueller, U. Wilhelm, J. Grotemeyer, Eur. Mass Spectrom. 1 (1995) 331.
[51] U. Wilhelm, Ch. Weickhardt, J. Grotemeyer, Rapid Commun. Mass Spectrom. 10 (1996) 473.
[52] D.A. Dahl, SIMION 3D, version 6.0, Princeton, NJ, 1995.
[53] V.M. Doroshenko, R.J. Cotter, J. Mass Spectrom. 33 (1998) 305.
[54] D.S. Cornett, M. Peschke, K. LaiHing, P.Y. Cheng, K.F. Wiley, M.A. Duncan, Rev. Sci. Instrum. 63 (1992) 2177.
[55] P.Y. Cheng, K.F. Wiley, J.E. Salcido, M.A. Duncan, Int. J. Mass Spectrom. Ion Processes 102 (1990) 67.
[56] D. Ioanoviciu, Rapid Commun. Mass Spectrom. 9 (1995) 985.
[57] U. Boesl, R. Weinkauf, C. Weickhardt, E.W. Schlag, Int. J. Mass Spectrom. Ion Processes 131 (1994) 87.
[58] X. Tang, R. Beavis, W. Ens, F. Lafortune, B. Schueler, K.G. Standing, Int. J. Mass Spectrom. Ion Processes 85 (1988) 43.
[59] S.V. Kovtoun, Rapid Commun. Mass Spectrom. 11 (1997) 433.
[60] S.V. Kovtoun, Rapid Commun. Mass Spectrom. 11 (1997) 810.
[61] D. Ioanoviciu, J. Am. Soc. Mass Spectrom. 6 (1995) 889.
[62] M. Amft, F. Moritz, Ch. Weickhardt, J. Grotemeyer, Rapid Commun. Mass Spectrom. 12 (1998) 1879.
[63] L.D. Hulett Jr., D.L. Donohue, T.A. Lewis, Rev. Sci. Instrum. 62 (1991) 2131.
[64] A.L. Rockwood, J.C.H. Sin, E.D. Lee, M.E. Gimon Kinsel, Proceedings of the 47th ASMS Conference on Mass Spectrometry, Dallas, 13–16 June 1999, paper TPC 055.
[65] C.A. Flory, R.C. Taber, G.E. Yefchak, Int. J. Mass Spectrom. Ion Processes 152 (1996) 169.
[66] R.W. Purves, L. Li, J. Am. Soc. Mass Spectrom. 8 (19977) 1085.
[67] R.W. Purves, W. Gabryelski, L. Li, Rapid Commun. Mass Spectrom. 12 (1998) 695.

[68] R.W. Purves, L. Li, J. Microcolumn. Sep. 7 (1995) 603.
[69] D. Ioanoviciu, Rapid Commun. Mass Spectrom. 12 (1998) 1925.
[70] T. Sakurai, T. Matsuo, H. Matsuda, Int. J. Mass Spectrom. Ion Processes 63 (1985) 273.
[71] T. Sakurai, H. Ito, T. Matsuo, Nucl. Instrum. Methods, Phys. Res. A 363 (1995) 426.
[72] T. Sakurai, H. Nakabushi, T. Hiasa, K. Okanishi, Nucl. Instrum. Methods, Phys. Res. A 427 (1999) 182.
[73] T. Sakurai, T. Matsuo, H. Matsuda, Int. J. Mass Spectrom. Ion Processes 68 (1986) 127.
[74] A.G. Ghielmetti, E.G. Shelley, Nucl. Instrum. Methods, Phys. Res. A 298 (1990) 181.
[75] H. Moestue, Rev. Sci. Instrum. 44 (1973) 1709.
[76] M.I. Yavor, H. Wollnik, M. Nappi, B. Hartmann, Nucl. Instrum. Methods, Phys. Res. A 311 (1992) 448.
[77] M.I. Yavor, B. Hartmann, H. Wollnik, Int. J. Mass Spectrom. Ion Processes 130 (1994) 223.
[78] P.P. Mahoney, S.J. Ray, G.M. Hieftje, Appl. Spectrosc. 51 (1997) 16A.
[79] A.N. Krutchinsky, A.V. Loboda, V.L. Spicer, R. Dworschak, W. Ens, K.G. Standing, Rapid Commun. Mass Spectrom. 12 (1998) 508.
[80] D.P. Myers, G. Li, P.P. Mahoney, G.M. Heftje, J. Am. Soc. Mass Spectrom. 6 (1995) 400.
[81] A.F. Dodonov, I.V. Chemushevich, V.V. Laiko, in Time-of-Flight Mass Spectrometry, R.J. Cotter (Ed.), ACS Symposium Series 549, Washington, DC, 1994, p. 108.
[82] J. Coles, M. Guilhaus, Trends Anal. Chem. 12 (1993) 203.
[83] M. Guilhaus, V. Mlynski, D. Selby, Rapid Commun. Mass Spectrom. 11 (1997) 951.
[84] J.M.B. Bakker, J. Phys. E 6 (1973) 785.
[85] H. Haberland, H. Kornmeier, C. Ludewigt, A. Risch, M. Schmidt, Rev. Sci. Instrum. 62 (1991) 2621.
[86] H. Haberland, H. Kornmeier, C. Ludewigt, A. Risch, Rev. Sci. Instrum. 62 (1991) 2368.
[87] C.K.G. Piyadasa, P. Hakansson, T.R. Ariyaratne, D.F. Barofsky, Rapid Commun. Mass Spectrom. 12 (1998) 1655.
[88] D.J. Beussman, P.R. Vlasak, R.D. McLane, M.A. Seeterlin, C.G. Enke, Anal. Chem. 67 (1995) 3952.